

All-optical switching in silicon-on-insulator photonic wire nano-cavities

Michele Belotti^{1,*}, Matteo Galli¹, Dario Gerace¹, Lucio Claudio Andreani¹, Giorgio Guizzetti¹, Ahmad R. Md Zain^{2,3}, Nigel P. Johnson², Marc Sorel² and Richard M. De La Rue²

1. Dipartimento di Fisica "A. Volta" and UdR CNISM, Università degli Studi di Pavia, Via Bassi 6, I-27100 Pavia, Italy

2. Optoelectronics Research Groups, Department of Electronics and Electrical Engineering, University of Glasgow, Rankine Building, Oakfield Avenue, Glasgow G12 8LT, UK

3. Photonics Research Group Centre for Communications Research (CCR) Department of Electrical and Electronic Engineering, University of Bristol, Queen's Building, Bristol BS8 1TR UK

* michele.belotti@unipv.it

Abstract: We report on experimental demonstration of all-optical switching in a silicon-on-insulator photonic wire nanocavity operating at telecom wavelengths. The switching is performed with a control pulse energy as low as ~ 0.1 pJ on a cavity device that presents very high signal transmission, an ultra-high quality-factor, almost diffraction-limited modal volume and a footprint of only $5 \mu\text{m}^2$. High-speed modulation of the cavity mode is achieved by means of optical injection of free carriers using a nanosecond pulsed laser. Experimental results are interpreted by means of finite-difference time-domain simulations. The possibility of using this device as a logic gate is also demonstrated.

© 2009 Optical Society of America

OCIS codes: (130.3750) Optical logic devices; (130.3120) Integrated optics devices; (130.5296) Photonic crystal waveguides (130.4815) Optical switching devices; (130.7408) Wavelength filtering devices; (230.1150) All-optical devices; (230.5750) Resonators; (230.5298) Photonic crystals.

References and links

1. J. Foresi, P. Villeneuve, J. Ferrera, E. Thoen, G. Steinmeyer, S. Fan, J. Joannopoulos, L. Kimerling, H. Smith, and E. Ippen, "Photonic-bandgap microcavities in optical waveguides," *Nature* **390**, 143 (1997).
2. D. Miller, "Rationale and challenges for optical interconnects to electronic chips," *Proceedings of IEEE* (IEEE, 2000), pp. 728–749.
3. Y. Vlasov, M. O'Boyle, H. Hamann, and S. McNab, "Active control of slow light on a chip with photonic crystal waveguides," *Nature* **438**, 65–69 (2005).
4. I. Märki, M. Salt, H. Herzig, R. Stanley, L. El Melhaoui, P. Lyan, and J. Fedeli, "Optically tunable microcavity in a planar photonic crystal silicon waveguide buried in oxide," *Opt. Lett.* **31**, 513–515 (2006).
5. H. Chong and R. De La Rue, "Tuning of photonic crystal waveguide microcavity by thermo-optic effect," *IEEE Photonics Technol. Lett.* **16**(6), 1528–1530 (2004).
6. Q. Xu, B. Schmidt, S. Pradhan, and M. Lipson, "Micrometre-scale silicon electro-optic modulator," *Nature* **435**, 325–327 (2005).
7. B. Schmidt, Q. Xu, J. Shakya, S. Manipatruni, and M. Lipson, "Compact electro-optic modulator on silicon-on-insulator substrates using cavities with ultra-small modal volumes," *Opt. Express* **15**, 3140–3148 (2007).

8. Q. Xu, S. Manipatruni, B. Schmidt, J. Shakya, and M. Lipson, "12.5 Gbit/s carrier-injection-based silicon micro-ring silicon modulators," *Opt. Express* **15**(2), 430–436 (2007).
9. S. Manipatruni, Q. Xu, and M. Lipson, "PINIP based high-speed high-extinction ratio micron-size silicon electrooptic modulator," *Opt. Express* **15**(20), 13035–13042 (2007).
10. K. Preston, S. Manipatruni, A. Gondarenko, C. Poitras, and M. Lipson, "Deposited silicon high-speed integrated electro-optic modulator," *Opt. Express* **17**(7), 5118–5124 (2009).
11. A. Liu, L. Liao, D. Rubin, H. Nguyen, B. Ciftcioglu, Y. Chetrit, N. Izhaky, and M. Paniccia, "High-speed optical modulation based on carrier depletion in a silicon waveguide," *Opt. Express* **15**(2), 660–668 (2007).
12. V. Almeida, C. Barrios, R. Panepucci, and M. Lipson, "All-optical control of light on a silicon chip," *Nature* **431**, 1081–1084 (2004).
13. T. Tanabe, M. Notomi, S. Mitsugi, A. Shinya, and E. Kuramochi, "All-optical switches on a silicon chip realized using photonic crystal nanocavities," *Appl. Phys. Lett.* **87**, 151112 (2005).
14. T. Tanabe, K. Nishiguchi, A. Shinya, E. Kuramochi, H. Inokawa, M. Notomi, K. Yamada, T. Tsuchizawa, T. Watanabe, H. Fukuda, *et al.*, "Fast all-optical switching using ion-implanted silicon photonic crystal nanocavities," *Appl. Phys. Lett.* **90**, 031115 (2007).
15. M. Soljacic and J. Joannopoulos, "Enhancement of nonlinear effects using photonic crystals." *Nat. Mater.* **3**(4), 211–219 (2004).
16. T. Tanabe, H. Taniyama, and M. Notomi, "Carrier Diffusion and Recombination in Photonic Crystal Nanocavity Optical Switches," *J. Lightwave Technol.*, **26**(11), 1396–1403 (2008).
17. P. Velha, E. Picard, T. Charvolin, E. Hadji, J. Rodier, P. Lalanne, and D. Peyrade, "Ultra-High Q/V Fabry-Perot microcavity on SOI substrate," *Opt. Express* **15**, 16090–16096 (2007).
18. A.R. Md Zain, M. Gnan, H. Chong, M. Sorel, and R. De La Rue, "Tapered Photonic Crystal Microcavities Embedded in Photonic Wire Waveguides with large Resonance Quality-Factor and High Transmission," *IEEE Photonics Technol. Lett.* **20**(1), 6–8 (2008).
19. A.R. Md Zain, N. Johnson, M. Sorel, and R. De La Rue, "Ultra high quality factor one dimensional photonic crystal/photonic wire micro-cavities in silicon-on-insulator (SOI)," *Opt. Express* **16**(16), 12084–12089 (2008).
20. S.F. Preble, V. Almeida, and M. Lipson, "Optically controlled photonic crystal nanocavity in silicon," *Proc. SPIE* **5511**, 10–17 (2004).
21. T. Tanabe, M. Notomi, H. Taniyama, and E. Kuramochi, "Dynamic Release of Trapped Light from an Ultrahigh-Q Nanocavity via Adiabatic Frequency Tuning," *Phys. Rev. Lett.* **102**, 043907 (2009)
22. P. Lalanne and J. Hugonin, "Bloch-wave engineering for high-Q, small-V microcavities," *IEEE J. Quantum Electron.* **39**(11), 1430–1438 (2003).
23. C. Sauvan, G. Lecamp, P. Lalanne, and J. Hugonin, "Modal-reflectivity enhancement by geometry tuning in Photonic Crystal microcavities," *Opt. Express* **13**(1), 245–255 (2005).
24. M. McCutcheon, G. Rieger, I. Cheung, J. Young, D. Dalacu, S. Frédérick, P. Poole, G. Aers, and R. Williams, "Resonant scattering and second-harmonic spectroscopy of planar photonic crystal microcavities," *Appl. Phys. Lett.* **87**, 221,110 (2005).
25. M. Galli, S. Portalupi, M. Belotti, L. Andreani, L. O'Faolain, and T. Krauss, "Light scattering and Fano resonances in high-Q photonic crystal nanocavities," *Appl. Phys. Lett.* **94**, 071101 (2009).
26. P. Deotare, M. McCutcheon, I. Frank, M. Khan, and M. Lončar, "High quality factor photonic crystal nanobeam cavities," *Appl. Phys. Lett.* **94**, 121106 (2009).
27. R. Soref and B. Bennett, "Electrooptical effects in silicon," *IEEE J. Quantum Electron.* **23**(1), 123–129 (1987).
28. M. Notomi, A. Shinya, S. Mitsugi, G. Kira, E. Kuramochi, and T. Tanabe, "Optical bistable switching action of Si high-Q photonic-crystal nanocavities," *Opt. Express* **13**, 2678–2687 (2005).
29. S. Leonard, H. van Driel, J. Schilling, and R. Wehrspohn, "Ultrafast band-edge tuning of a two-dimensional silicon photonic crystal via free-carrier injection," *Phys. Rev. B* **66**, 161102 (2002).
30. M. Belotti, J. Galisteo López, S. De Angelis, M. Galli, I. Maksymov, L. Andreani, D. Peyrade, and Y. Chen, "All-optical switching in 2D silicon photonic crystals with low loss waveguides and optical cavities," *Opt. Express* **16**(15), 11624–11636 (2008).
31. Q. Xu and M. Lipson, "All-optical logic based on silicon micro-ring resonators," *Opt. Express* **15**(3), 924–929 (2007).
32. F. Doany, D. Grischkowsky, and C. Chi, "Carrier lifetime versus ion-implantation dose in silicon on sapphire," *Appl. Phys. Lett.* **50**, 460 (1987).
33. M. Först, J. Niehusmann, T. Plötzing, J. Bolten, T. Wahlbrink, C. Moormann, and H. Kurz, "High-speed all-optical switching in ion-implanted silicon-on-insulator microring resonators," *Opt. Lett.* **32**, 2046–2048 (2007).
34. K. Preston, P. Dong, B. Schmidt, and M. Lipson, "High-speed all-optical modulation using polycrystalline silicon microring resonators," *Appl. Phys. Lett.* **92**, 151104 (2008).
35. M. Waldow, T. Plötzing, M. Gottheil, M. Först, J. Bolten, T. Wahlbrink, and H. Kurz, "25 ps all-optical switching in oxygen implanted silicon-on-insulator microring resonator," *Opt. Express* **16**(11), 7693–7702 (2008).
36. K. Sokolowski-Tinten and D. von der Linde, "Generation of dense electron-hole plasmas in silicon," *Phys. Rev. B* **61**, 2643–2650 (2000).
37. T. G. Euser and W. L. Vos, "Spatial homogeneity of optically switched semiconductor photonic crystals and of

1. Introduction

One of the major topics of interest in recent photonic research is the study and development of micro- and nano-structures for fast signal processing in the telecom window. These structures are required to be compact and compatible with monolithic integration into a single CMOS chip. The combination of one-dimensional photonic crystal (PhC) structures with narrow waveguides in high refractive index contrast materials, such as silicon-on insulator (SOI), can satisfy all the requirements [1, 2].

Switching devices are essential components for processing of the signal when designing an all-optical integrated circuit (IC). Although a few proposals have been demonstrated based on non-optical modulation mechanisms, such as thermo-optic [3–5] or electro-optic [6–10] control, it is widely acknowledged that all-optical switching is the most promising technology towards the achievement of faster response times in signal processing. Unfortunately, the optical nonlinearities commonly used to modulate the signal are weak in Silicon, thus requiring large interaction lengths, as in devices like Mach-Zehnder interferometers [11], or sizeable operational powers. As it has been shown in a number of papers [12–14], the problem can be solved by using optical resonators, which are able to enhance light-matter interaction. This strengthened interaction makes it possible to exploit weak optical pump pulses to induce a significant resonance shift for a probe beam, thus achieving all-optical switching operation. For this purpose, PhC cavities are very promising, thanks to their high quality factors (Q) and small modal volumes (V), which allow for strong light-matter interaction on sub-wavelength length scales. On one hand, the maximum light intensity inside the cavity is proportional to the ratio $1/V$, on the other, the required wavelength shift to obtain full switching is proportional to $1/Q$. The overall effect is a reduction of the power required to switch the signal by a factor Q/V , which can be very large in a PhC nanocavity. The switching power can be even proportional to Q^2/V if both probe and pump beams are resonant with the cavity modes [15]. It thus becomes feasible to achieve an all-optical switching component working with a low enough control power to be integrated on a chip. The physical volume of the cavity has an important effect on the device commutation speed as well, because the relaxation time depends on the size when dealing with carrier-induced refractive index variations [16]. Furthermore, it is very important to achieve such interaction strengths in a system that presents the highest possible transmission, together with reduced losses, which is required for efficient processing of the signal. As compared to earlier pioneering work on this subject [12–14], a device having all these characteristics at the same time is still being developed.

Recently, high- Q PhC nanocavities in photonic wire (PhW) waveguides made of SOI were successfully demonstrated [17–19]. Photonic wire waveguide mirrors, that consist of a periodic array of holes realized in a silicon wire on a silicon dioxide cladding layer, have very low propagation losses in a mechanically more robust system as compared to air-bridge structures. Nanocavities in photonic wires yield very high quality factors with low modal volumes: they are, therefore, good candidates for applications as integrated photonic devices with small footprint, high mechanical stability, and strong enhancement of radiation-matter interaction. In the present work we show all-optical switching in PhC/PhW nanocavities, in which large absolute transmission and low switching power can be obtained simultaneously in a very compact, integrable and CMOS compatible nano-structure. After a preliminary characterization of the linear optical response by means of waveguide transmission, in which we show transmittance values as high as $\sim 40\%$, all-optical switching is demonstrated with a very low control power of ~ 120 fJ. One-photon free-carrier generation in a configuration similar to that of [12, 20, 21] is the physical mechanism employed to modify the optical response of the high- Q cavity mode.

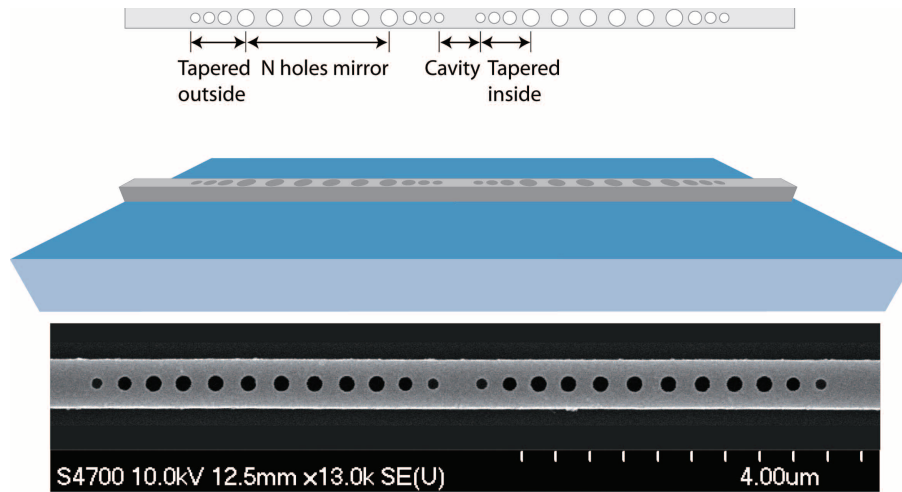


Fig. 1. Sketch and scanning electron micrograph (SEM) image of the tapered PhC cavity embedded in a PhW waveguide with two mirrors composed by periodically spaced holes and aperiodic taper region inside and outside the cavity. The cavity in SEM picture has 6 holes in each mirror spaced by 350 nm and identical aperiodic taper region inside and outside. The spacings between adjacent holes are 300, 315, and 325 nm respectively. The corresponding hole radii are 65, 80, 85 nm.

Finally, we also demonstrate the possibility of performing various gate operations by carefully tuning the probe wavelength with respect to the cavity resonance.

The paper is structured as follows: In Sec. 2 we describe the design and the fabrication of the device. In Sec. 3 we report the FDTD simulations. In Sec. 4 the linear, the resonant scattering characterization and the all-optical switching of the device is reported. We also describe the all-optical logic operation that can be performed with our sample. In Sec. 5 we summarize the main results of the work.

2. Sample description

The samples employed in the present work were fabricated by using electron beam lithography and reactive ion etching techniques on SOI wafers (obtained from SOITEC™) having a 260 nm silicon core layer supported by a 1 μm silica layer. The device is realized within a 1D PhC/PhW nanocavity structure consisting of a single row of circular holes embedded in a 500 nm wide PhW waveguide with a lattice constant $a = 350$ nm and $r/a = 0.28$. The photonic crystal mirror is designed to exhibit a large stop band center around 1550 nm for TE polarization. To reduce the out-of-plane scattering, i.e. to increase simultaneously the cavity mode Q-factor and the absolute transmittance of the system, the mismatch between the waveguide modal effective index ($n_{wg} = 2.9$) and the Bloch mode index ($n_B = 2.07$) is adiabatically reduced through proper cavity design. The regions within the cavity and between the mirrors and the waveguide are carefully tapered by means of holes with different diameters and significantly aperiodic spacings [22, 23], which makes it possible to reduce and recycle the mirror losses due to out-of-plane scattering induced by optical impedance mismatch. Different cavity lengths with different mirror hole numbers and taper geometries have been realized in order to enhance the Q factor, while simultaneously maintaining a useful optical transmission level. A sketch of the cavity with the two mirrors and tapers is presented in Fig. 1 with a scanning electron micrograph (SEM) image of a fabricated device. The figure shows a 500 nm wide photonic

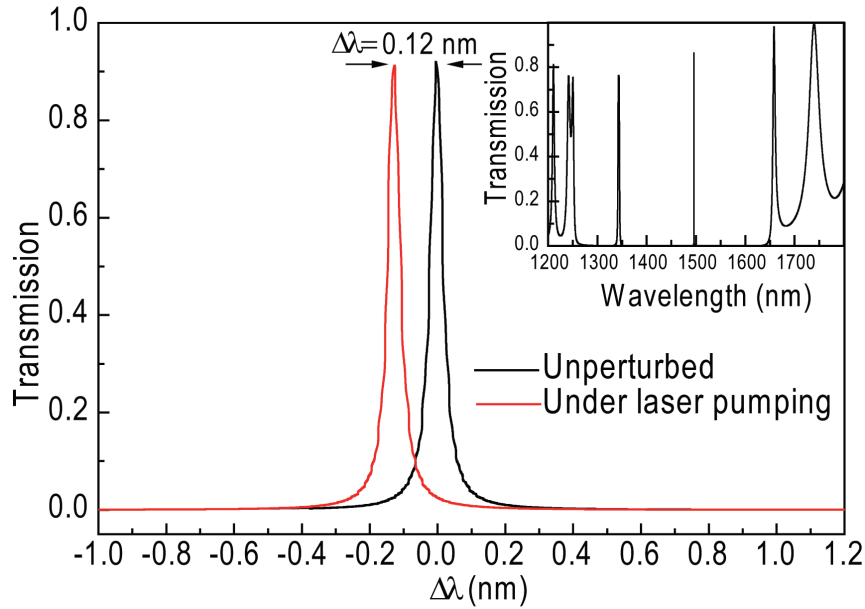


Fig. 2. Simulated transmission spectra of the device without (black curve) and with (red curve) the pump pulse. The simulated blue-shift is 0.12 nm. In the right inset, a broad-band spectrum is given, showing the cavity resonance within the 1D photonic band gap.

wire nanocavity formed by two mirrors, each of which includes a periodic array of six holes with the same diameter. Gradually tapered hole arrangements with different spacing and diameters are used inside and outside the cavity (three holes in each taper region, yielding a total of 12 holes in each mirror). The whole structure is very compact and we can estimate the total device footprint to be $10\mu\text{m}$ (length of the cavity plus the mirrors) $\times 0.5\mu\text{m}$ (waveguide width) = $5\mu\text{m}^2$. Simulations show that the resonant modal area is much smaller than the footprint (see next paragraph).

The waveguide patterns were defined using a hydrogen silsesquioxane (HSQ) negative-tone resist spun at 3000 rpm to give 200 nm in thickness. The devices were fabricated using single-step direct-write electron beam lithography in a Vistec VB6 machine at 100 keV electron energy, with proximity correction at a base dose of $1500\mu\text{C}/\text{cm}^2$ [18]. This VB6 beam writer has the capability of writing a 1.2 mm by 1.2 mm field at 1.25 nm resolution. In addition, extra care has to be taken to reduce the potentially significant impact of field stitching errors on the pattern produced - i.e. to ensure the flatness of the sample during the writing process. The patterns were finally transferred into the silicon guiding layer by using an inductively-coupled plasma (ICP) etching machine from the STS company. $\text{SF}_6/\text{C}_4\text{F}_8$ combined chemistry was used to etch the silicon layer, leading to the creation of silicon waveguides with smooth side-walls. The silicon layer is etched for 49 seconds with a silicon etching rate of 5 nm/s and Si/SiO₂ selectivity of ~ 10 .

3. Simulations

The simulated linear transmission spectra and spatial distribution of the electromagnetic field for the structure presented in Fig. 1 are shown in Fig. 2, as obtained by using a 2D Finite Difference Time-Domain (FDTD) solver. In particular, this structure is made of a 6 holes mirror, together with 3 holes to taper both the mirror and the cavity, which has 425 nm long spacer

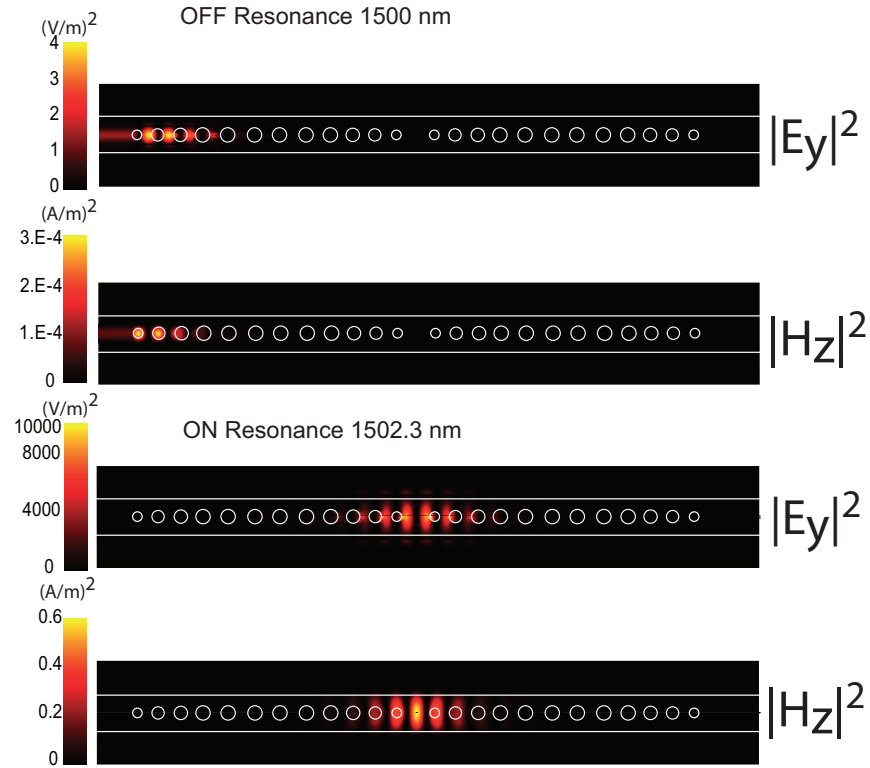


Fig. 3. The calculated field intensities at resonance (1502.3 nm) and off resonance (1500 nm) are shown for the $|E_y|^2$ and $|H_z|^2$ component, respectively. Notice the change in scales from off to on resonance.

section (taken from edge-to-edge of the side holes). The spacing between adjacent holes and the hole radii in the taper region are 300, 315, 325, 65, 80, 85 nm, respectively. The fundamental transverse-electric (TE) guided mode of the PhW waveguide is used as an input propagating pulse to study the device transmittance. We first estimated the propagation waveguide mode in the wire waveguide (3D mode solver) and we obtain an effective index of $n_{eff} = 2.915$. We then used such n_{eff} for the 2D FDTD simulation of the transmission experiment. A local change in the refractive index of the silicon material around the cavity region is used to simulate the effects of free carrier injection induced by laser pumping at frequencies above the silicon gap. The calculated spectra in Fig. 2 display a high-transmission ($\sim 90\%$) resonance at 1502.3 nm for the unperturbed structure, and a 0.1 nm blue-shifted one for the pumped structure. The latter has been simulated with the silicon refractive index reduced by 0.01% (corresponding to a free carriers injection of $4.8 \cdot 10^{16} \text{cm}^{-3}$) in a $10 \mu\text{m}$ -wide linear region centered around the cavity (to mimic the focused laser spot onto the silicon wire). In both cases, the calculated Q-factor can be estimated to approach 10^5 . The field intensity for the $|E_y|^2$ and $|H_z|^2$ components is reported in Fig. 3 for off- and in- resonance case, respectively. Out of resonance, at the wavelength of 1500 nm, the light traveling into the guide penetrates the first holes composing the mirror and it is completely reflected backwards. For the resonance case light passes through the mirror and the field is localized in the cavity region. Also the field intensities at resonance are enhanced by $\sim 10^4$ as compared to the off-resonance case, as it can be seen from the figure. A 3D FDTD simulation of the cavity mode profile, with excitation by an internal dipole source, gives an

effective mode volume $V_{eff} = \int \epsilon(\mathbf{r})|\mathbf{E}(\mathbf{r})|^2 d\mathbf{r} / \max\{\epsilon(\mathbf{r})|\mathbf{E}(\mathbf{r})|^2\} \simeq 0.1\mu\text{m}^3 \sim 1.24(\lambda/n)^3$, i.e., the mode volume is very small and close to the diffraction limit, implying strong reduction of power density required for all-optical switching.

4. Experimental results

Experimental linear transmission is measured with a continuous wave tunable laser delivered onto the optical set-up by a single-mode polarization maintaining fibre. The incident probe beam is polarized along the plane of periodicity (TE polarization). It is focussed into and collected from the access ridge waveguides by a pair of high numerical aperture objective lenses. The collected signal is then spatially filtered by a single mode optical fiber and by an analyzer to remove spurious substrate guided light. The light is then detected by an amplified InGaAs photodiode connected to a lock-in amplifier. The experimental results were normalized with respect to an identical, but unpatterned, 500 nm wide wire waveguide. The cavity is also characterized by means of crossed-polarization resonant scattering technique [24, 25]. Light from the tunable laser is linearly polarized by a polarizer and focused on the cavity by a high numerical aperture objective. The reflected beam is analyzed by a second polarizer with its polarization axis orthogonal to the first one.

In Fig. 4(a), we show the measured linear transmittance of a fabricated PhC/PhW nano-cavity sample having the same nominal parameters as the structure simulated in Fig. 2. The spectrum shows a strong resonance for the wavelength $\lambda=1483.16$ nm with a high signal/background ratio. The inset shows a higher resolution spectrum of the resonance that was used to determine the Q-factor. From the Full-Width Half-Maximum of 16.6 pm we can estimate a loaded Q-factor value of 89,300 corresponding to a photon lifetime of ~ 67 ps. Normalizing the transmission to the unstructured guide, we estimate a transmission coefficient of about 38%. The same cavity was also characterized by the resonant scattering technique, i.e. normal incidence reflectance with crossed polarizations [24]. The measured spectrum is reported in Fig. 5. The spectrum presents a very sharp resonance at the same wavelength as observed in the transmission experiment, due to the change in polarization induced by the coupling of the incident light with the cavity [26]. By fitting the resonance with a Fano lineshape [25] (red curve in Fig. 5) we can estimate an cavity Q factor of about 120,000 corresponding to a photon lifetime of ~ 97 ps. The different values of the quality factor are mainly due to two-photon absorption in the cavity in the transmission experiment. In fact the amount of light power coupled to the cavity is higher in the transmission experiment than in resonant scattering one. So in the transmission experiment the two-photon absorption mechanism plays the role of a loss channel, reducing the resonance quality factor.

In Fig. 4(b) we show the linear transmittance of a second device with identical geometrical parameters, except for the cavity length, which is 425 nm. Also in this case we can observe a strong resonance at a slightly different wavelength (1502.3 nm) with roughly the same transmission level (about 39 %). From a lorentzian fit we can estimate a FWHM of 23.8 pm that corresponds to a Q-factor of about 63,000, slightly lower than in the first device. By changing the cavity length it is possible to tune the resonance without significant changes in the transmission behavior.

For the switching experiments, optical pumping is performed with a frequency doubled Q-switched Nd:YAG laser at a wavelength of 532 nm with a pulse width of 2.5 ns and a repetition rate of 11 kHz. The pump beam is focused normally to sample surface in a $5\mu\text{m}$ spot around the optical cavity using a microscope objective. The pump impinging on the surface generates free carriers optically, which lowers the refractive index of the silicon backbone [12, 27–31]. The pump beam modifies the optical response of the sample only very close to the cavity region, hence reducing the required power to control the transmittance. The transmitted probe

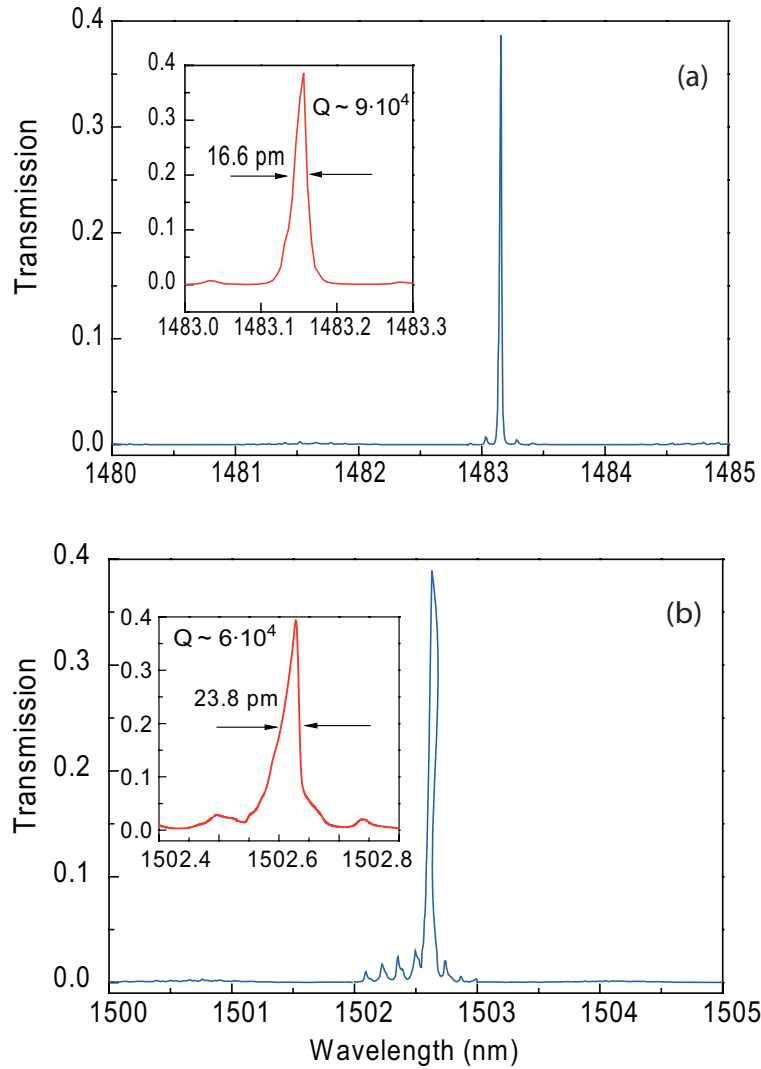


Fig. 4. Transmission spectrum for the sample with 6 holes mirror, 3 holes taper inside and outside the cavity, cavity length of (a) 400 nm and (b) 425 nm, respectively. (a) The spectrum shows a resonance for the wavelength 1483.16 nm with a Q-factor of approximately 89,300. (b) The spectrum shows a strong resonance with a Q-factor of about 63,000 for the wavelength of 1502.3 nm.

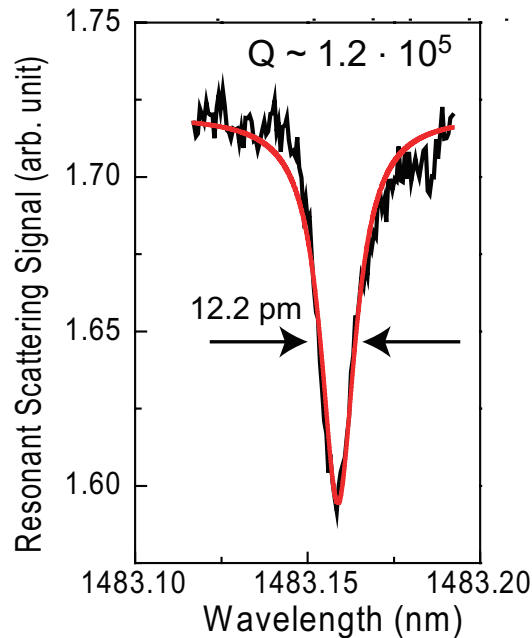


Fig. 5. Resonant scattering spectrum of the sample with 6 holes mirror, 3 holes taper inside and outside the cavity, cavity length of 400 nm. The red curve is the Fano lineshape best-fit.

signal collected by the avalanche InGaAs detector when pumping the sample is amplified with a voltage amplifier and registered by an oscilloscope operating with 1 GHz bandwidth. Part of the original pump beam is diverted from pump line and used to trigger the oscilloscope. In order to record the switching of the resonance, we track the temporal evolution of the probe beam transmittance at a fixed wavelength (λ_p) as a function of the pump pulse delay. This operation is repeated for different wavelengths around the cavity mode resonance. Although a pumping scheme with a frequency below that corresponding to the silicon bandgap energy and a pump beam propagating in the waveguide [13] are more suitable for the realistic operation of a fully integrated functional device, the present setup also has definite advantages since there is no need for the cavity design to support more than one resonance. Moreover the time-resolved cavity response can be linked directly to the pump pulse, which does not suffer from possible delay and broadening in waveguide propagation. Notice that in the present pumping configuration the cavity enhancement is proportional to Q/V and that a similar pumping configuration has been used in [12, 21] for the study of optical switching and adiabatic tuning of cavity modes, respectively.

In Fig. 6(a) we show the switching behavior of the sample of Fig. 4(a) driven by the pump beam, with the probe beam set on resonance ($\Delta\lambda = 0$ nm) and with the cavity mode amplitude normalized at the cavity transmission. For a time shorter than the rise time of the pump pulse, no change is observed in the transmitted intensity. In coincidence with the arrival of the pulse, we see a dramatic drop in transmission that is a consequence of the resonance blue shift induced by the change of the refractive index in the cavity region. The temporal width of the transmission drop equals that of the pump pulse (2.5 ns), as shown in Fig. 6(c), indicating that all generated free carriers recombine in a time scale that is shorter than our experimental temporal resolution. This is compatible with the recovery time reported in previous work on silicon PhC waveguide

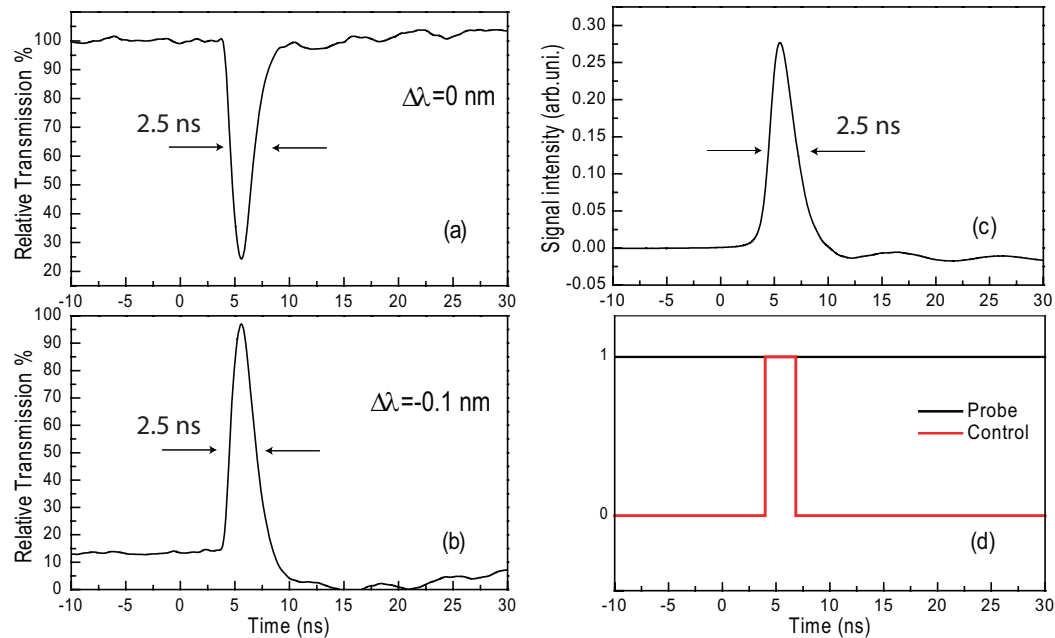


Fig. 6. Time evolution of switching logic operation: (a) NOT operation: the output is high (on-condition) when the control level is low and it switches to low (off-condition) when the control level becomes high. (b) AND operation: the output is low (off-condition) when the control level is low, and it is high (on-condition) when the control is high. (c) Pump intensity as a function of time. The pulse width is 2.5 ns. (d) Scheme of the applied probe and control beam.

devices [14, 16, 32–35]. Notice that a photon lifetime $\tau = 67$ ps in the present transmission configuration is much below experimental resolution. Together with the free carrier lifetime, the cavity photon lifetime sets a limit for the switching speed in the present device.

The latter configuration, i.e. when the probe is tuned on resonance, corresponds to performing a NOT logic operation, where the control pulse acts as a logic 1 input. The output signal is low only when the control pulse beam is high, i.e. the output is exactly the reciprocal signal of the pump control. Repeating the same procedure for a probe wavelength slightly lower than the resonance wavelength ($\Delta\lambda = -0.1$ nm), we can recover the situation shown in Fig. 6(b). In the latter case, the transmission is zero before the pulse occurs, due to the wavelength filtering performed by the cavity. The transmission increases in coincidence with the pulse due to a blue shift of the cavity mode, yielding a resonance condition with the probe wavelength. After the pulse the signal drops to zero, thereby restoring the initial condition. In this situation we operate a different logic operation that corresponds to an AND gate: only when both inputs are high does the output turn high. A sketch of the logic signals is shown in Fig. 6(d).

Furthermore, taking the temporal behavior at different probe wavelengths (same experimental conditions and normalization procedure as in Fig. 4) makes it possible to reconstruct fully the time dependence of the spectra, as shown in Fig. 7(a) where the temporal transmission change recorded at a fixed wavelength is added to the unperturbed transmittance value at the same wavelength. We also observe, in this case, complete switching during the pulse peak, dominated by the intrinsic time length of the pulse. We can appreciate this more clearly by examining Fig. 7(b), where we trace the temporal shift behavior of the wavelength $\Delta\lambda_{\max}$ of

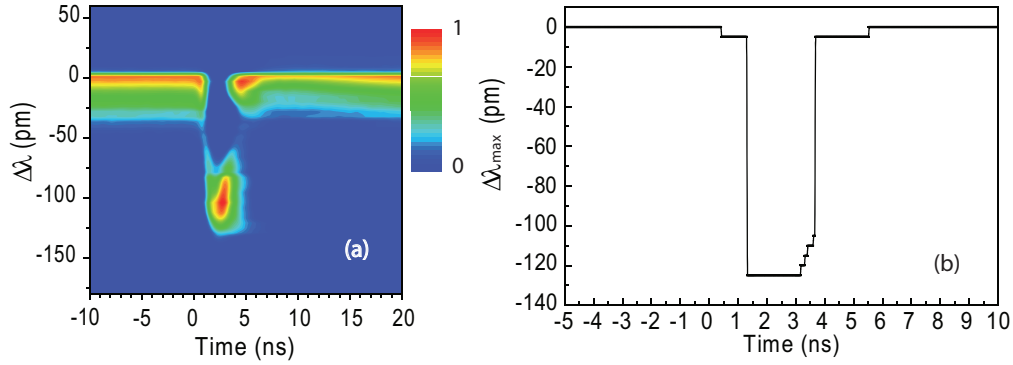


Fig. 7. (a) Time resolved evolution of the transmission spectrum when a pump with 2.5 ns duration and 2 pJ energy is applied. The normalized intensity color scale is in linear units. (b) Extracted shift $\Delta\lambda$ of the resonance wavelength as a function of time.

the resonance maximum extracted from Fig. 7(a). The distinctly stepped behavior is further evidence that all the processes involved (change in the refractive index, free carrier recombination) are faster than our time window. From both figures we can evaluate the shift of the resonance, which is estimated to be ~ 0.12 nm.

The calculated carrier concentration produced by the laser pump fluence can be estimated from the intensity profile of the pump laser beam in the material [37]:

$$N_{eh} = \int \frac{I(z)\tau_{\text{pump}}}{\hbar\omega_{\text{pump}}} \left[\alpha + \frac{1}{2}\beta I(z) \right] dz$$

where $I(z)$ is the intensity profile calculated from the absorption of silicon (the penetration depth is about 800 nm for light at 532 nm), α is the linear absorption coefficient, β the two-photon absorption coefficient, τ_{pump} the pulse width and $\hbar\omega_{\text{pump}}$ the light energy. Solving the integral on the silicon thickness we obtain a carrier density of $4.8 \times 10^{16} \text{ cm}^{-3}$. The corresponding refractive index variation in the silicon material is calculated through the Drude contribution: [27, 36]:

$$\varepsilon(\omega) = \varepsilon_B(\omega) + \Delta\varepsilon_{eh}(\omega) = \varepsilon_B(\omega) - \left(\frac{\omega_p}{\omega} \right)^2 \frac{1}{1 + \frac{i}{\omega\tau_D}}$$

being τ_D the Drude damping time. The carrier density enters the dielectric function variation through the plasma frequency:

$$\omega_p = \sqrt{\frac{N_{eh}e^2}{\varepsilon_0 m_e m_{opt}}}$$

where e is the electronic charge, N_{eh} the free carrier density, m_e is the electron mass and m_{opt} is the optical effective mass of the carriers in units of the electron mass. If one assumes a density of generated free carriers $N_{eh} < 10^{22} \text{ cm}^{-3}$, it can be shown [37] that the change in refractive index of silicon is given by:

$$n = n_0 - \frac{e^2}{2n_0\varepsilon_0 m_{opt} m_e \omega^2} N_{eh}.$$

In our calculations, the numerical values for m_{opt} and τ_D were taken from Ref. [37]. The calculated index variation is $n \approx -0.01\%$. The energy required for all-optical switching is estimated as follows. The pump laser beam focused onto the nano-cavity has an average power of 21 nW

and a pulse energy $E=2$ pJ. It is focused to a spot of approximately $10\ \mu\text{m}$ diameter, which corresponds to an power density of $0.97\ \text{kW}/\text{cm}^2$. However, only a fraction of the incident beam excites free carriers in the Si wire. Estimating an excited area of $10\ \mu\text{m} \times 0.5\ \mu\text{m}$, and taking the ratio between the excited area and the wire area, the incident energy in the wire is ~ 124 fJ. This value should be considered as a conservative estimate, since significant amounts of the power incident on the wire will be either reflected at the silicon-air interface or transmitted at the silicon core-silica cladding interface. Please note that the light penetration depth at $532\ \text{nm}$ is about $800\ \text{nm}$, larger than the thickness of the device. The shift observed in Fig. 7 is very well reproduced by an FDTD simulation with the same index reduction as previously shown in Fig. 2, thereby validating the previous estimation.

While the present experiments are performed in a configuration with a control beam incident from the top surface and with a cavity designed for a single resonance, it is interesting to explore the possibility of employing a cavity supporting two resonances (especially with both modes in the telecom window) and designing the whole device for in-plane control beam configuration. This can be done by designing a longer cavity and/or coupled photonic cavities. In both cases the device footprint is expected to increase by at most a cavity length or a few periods of the Bragg mirrors, i.e., by a length of the order of a micron. The slight increase in mode volume would be more than compensated by the scaling of the switching power like Q^2/V (rather than like Q/V in the present experiment). Thus, the present high-Q cavities in silicon-on-insulator photonic wires are very promising for the design of fully integrated all-optical switches with a small footprint.

5. Conclusions

All-optical switching with a very low operating power has been demonstrated on high quality-factor photonic crystal/photonic wire nano-cavities fabricated in silicon-on-insulator, with high transmissivity and very low modal volume, at wavelengths in the telecom range. This system, based on an SOI platform, is mechanically robust, since it does not employ suspended membrane waveguides - and can provide full optical functionality within a total footprint of only $5\ \mu\text{m}^2$. The energy delivered to the silicon photonic wire that is required to obtain full switching with at least a $10\ \text{dB}$ on-off ratio is as low as 120 fJ. We have also demonstrated the feasibility of operation as a logic gate with different functional configurations.

Acknowledgments

This work was supported by the Fondazione CARIPO under project n. 2007-5259, by the Italian Ministry of Universities and Research through FIRB contract #RBAP06L4S5 and by the Malaysian Ministry of Education and Science. We are also grateful for the use of the facilities of the James Watt Nanofabrication Centre (JWNC) at the University of Glasgow.